

Major Cluster Mergers and the Location of the Brightest Cluster Galaxy

Hugo Martel^{1,2} Fidèle Robichaud,^{1,2} and Paramita Barai³

ABSTRACT

Using a large N-body cosmological simulation combined with a subgrid treatment of galaxy formation, merging, and tidal destruction, we study the formation and evolution of the galaxy and cluster population in a comoving volume $(100 \text{ Mpc})^3$ in a Λ CDM universe. At $z = 0$, our computational volume contains 1788 clusters with mass $M_{\text{cl}} > 1.1 \times 10^{12} M_{\odot}$, including 18 massive clusters with $M_{\text{cl}} > 10^{14} M_{\odot}$. It also contains 1 088 797 galaxies with mass $M_{\text{gal}} \geq 2 \times 10^9 M_{\odot}$ and luminosity $L > 9.5 \times 10^5 L_{\odot}$. For each cluster, we identified the brightest cluster galaxy (BCG). We then computed two separate statistics: the fraction f_{BNC} of clusters in which the BCG is not the closest galaxy to the center of the cluster in projection, and the ratio $\Delta v/\sigma$, where Δv is the difference in radial velocity between the BCG and the whole cluster, and σ is the radial velocity dispersion of the cluster. We found that f_{BNC} increases from 0.05 for low-mass clusters ($M_{\text{cl}} \sim 10^{12} M_{\odot}$) to 0.5 for high-mass ones ($M_{\text{cl}} > 10^{14} M_{\odot}$), with very little dependence on cluster redshift. Most of this turns out to be a projection effect, and when we consider 3D distances instead of projected distances, f_{BNC} increases only to 0.2 at high cluster mass. The values of $\Delta v/\sigma$ vary from 0 to 1.8, with median values of in the range 0.03–0.15 when considering all clusters, and 0.12–0.31 when considering only massive clusters. These results are consistent with previous observational studies, and indicate that the central galaxy paradigm, which states that the BCG should be at rest at the center of the cluster, is usually valid, but exceptions are too common to be ignored. We built merger trees for the 18 most massive clusters in the simulation. Analysis of these trees reveal that 16 of these clusters have experienced one or several major or semi-major mergers in the past. These mergers leave each cluster in a non-equilibrium state, but eventually the cluster settles into an equilibrium configuration, unless it is disturbed by another major or semi-major merger. We found evidence that these mergers are responsible for the off-center positions and peculiar velocities of some BCGs. Our results thus support the merging-group scenario, in which some clusters form by the merger of smaller groups in which the galaxies have already formed, including the galaxy destined to become the BCG. Finally, we argue that f_{BNC} is not a very robust statistics, being very sensitive to projection and selection effect, but that

¹Département de physique, génie physique et optique, Université Laval, Québec, QC, G1V 0A6, Canada

²Centre de Recherche en Astrophysique du Québec, QC, Canada

³INAF-Osservatorio Astronomico di Trieste, Trieste, Italy

$\Delta v/\sigma$ is a more robust one. Still, both statistics exhibit a signature of major mergers between clusters of galaxies.

Subject headings: galaxies: clusters: general — galaxies: general — methods: numerical

1. Introduction

Clusters of galaxies contain hundreds or thousands of galaxies with a full range of luminosities, going from low-luminosity dwarf galaxies to L^* galaxies and beyond. If clusters are dynamically relaxed systems, we naturally expect the brightest galaxies, which are presumably the most massive ones, to be concentrated in the central regions of clusters, since this is the most stable configuration. In particular, in each cluster, we expect to find the brightest galaxy cluster (BCG) at rest at the center.¹ van den Bosch et al. (2005) refer to this assumption as the “central galaxy paradigm.”

This paradigm has played an important role in the development of semi-analytical models of galaxy formation over the past twenty years. In the early model of Kauffmann et al. (1993), each dark matter halo can host a central galaxy plus a number of satellite galaxies. In the initial state, halos contain only a mixture of cold and hot gas, with no galaxy. Eventually, a central galaxy forms at the center of each halo. Then, when a merger between several halos takes place, the central galaxy of the most massive progenitor becomes the central galaxy of the new halo, while all other galaxies become satellite galaxies. In this model, the brightest galaxy in a halo is always the central one. Many other semi-analytical models of galaxy formation have been developed since, and the central galaxy paradigm remains a key ingredient for most of them (Cole et al. 2000; Hatton et al. 2003; Baugh 2006; Monaco et al. 2007; Somerville et al. 2008), though some models locate the central galaxy at the minimum of the gravitational potential (Springel et al. 2001; Croton et al. 2006; Guo et al. 2011), which can be off-center if the halo contains substructures. Halo occupation modeling (Scoccimarro et al. 2001; Sheth et al. 2001; Yang et al. 2003; Zehavi et al. 2005; Zheng et al. 2005; Cooray 2005; Phleps et al. 2006; van den Bosch et al. 2007; Tinker et al. 2008; Reid & Spergel 2009; Matsuoka et al. 2011; Richardson et al. 2012) and large N-body simulations of structure formation in CDM universes (Taylor & Babul 2004; Springel et al. 2005; De Lucia & Blaizot 2007) also rely on the assumption that the brightest galaxy is located in the center of the parent halo.

Several studies assume a phenomenological model that a massive “central” galaxy lies at the center of the host dark matter halo, and “satellites” constitute of the remaining galaxies in the halo (as in Kauffmann et al. 1993). Observations attempt to quantify the correlations and differences between the properties (like SFR, color) of central and satellite galaxy populations, and their dependence on the environment (Weinmann et al. 2006; Azzaro et al. 2007; Kimm et al. 2009;

¹In the literature, this galaxy is called either the *Brightest Halo Galaxy* (BHG), *Brightest Cluster Galaxy* (BCG), or *Brightest Cluster Member* (BCM). All terms are equivalent. In this paper, we use BCG.

Prescott et al. 2011; Wetzel et al. 2013; Woo et al. 2013; Yang et al. 2013). Also, many observational techniques are based on the assumption that the central galaxy paradigm is valid. These include measurement of halo masses by satellite kinematics (McKay et al. 2002; van den Bosch et al. 2004; More et al. 2009; Romanowsky et al. 2009; Dutton et al. 2010; Watson et al. 2012), weak lensing (Mandelbaum et al. 2006; Johnston et al. 2007; Cacciato et al. 2009; Sheldon et al. 2009; Pastor Mira et al. 2011; van Uitert et al. 2012; Li et al. 2013), and strong lensing (Kochanek 1995; Cohn et al. 2001; Koopmans & Treu 2003; Rusin et al. 2003; Oguri 2006; Killedar et al. 2012; More et al. 2012), and automated identification of groups and clusters in redshift surveys (Yang et al. 2005, 2007; Berlind et al. 2006; Koester et al. 2007).

Observational studies of galaxy clusters have been performed in order to test the validity of the central galaxy paradigm (Beers & Geller 1983; Malumuth et al. 1992; Zabludoff et al. 1993; Bird 1994; Postman & Lauer 1995; Zabludoff & Mulchaey 1998; Oegerle & Hill 2001; Yoshikawa et al. 2003; Lin & Mohr 2004; von der Linden et al. 2007; Bildfell et al. 2008; Hwang & Lee 2008; Sanderson et al. 2009; Coziol et al. 2009; Skibba et al. 2011). Two different approaches are used in these studies. The first one consists of measuring the difference in radial velocity between the BCG and the cluster itself, and comparing it to the velocity dispersion of the cluster. The second one consists of measuring the projected distance between the BCG and the center of the cluster, estimated either from the distribution of galaxies or from the peak X-ray luminosity. The overall conclusion is that the central galaxy paradigm is usually valid, that is, most BCGs are at rest at the center of their host cluster, but many of them are not, too many to be dismissed as peculiar objects. In two of the most recent studies, Coziol et al. (2009) studied a large sample of clusters containing 1426 candidate BCGs, and found that a significant number of BCGs have large peculiar velocities, the median value being 32% of the radial velocity dispersion of the cluster. Skibba et al. (2011) studied a sample of 334 010 galaxies from the *Sloane Digital Sky Survey* (SDSS), and found that the fraction f_{BNC} of clusters in which the brightest galaxy is not the central one varies from 0.25 for low-mass clusters to 0.40 for high-mass one. In both papers, the authors suggest that major mergers between clusters might explain their results. The central galaxy paradigm is based on the assumption that the galaxies inside a parent cluster either formed concurrently with the cluster, or later, after the distribution of dark matter and gas in the cluster had settle into an equilibrium configuration (Ostriker & Tremaine 1975; Haussman & Ostriker 1978; Merritt 1984; Malumuth 1992). One alternative scenario is that the cluster formed by the merger of smaller groups (Malumuth 1992; Ellingson 2003; Mihos 2004; Adami et al. 2005; Adernach & Coziol 2007; Coziol & Plauchu-Frayn 2007), and that the galaxy that will eventually become the BCG already existed in one of these groups (Merritt 1985; Bird 1994; Zabludoff & Mulchaey 1998; Pimbblet et al. 2006). If the cluster has not yet reached equilibrium by the present, this could explain the off-center location and peculiar velocity of the BCG.

Our goal is to test this *Merging-Group Scenario*, as Coziol et al. (2009) call it. We performed a numerical simulation of the formation and evolution of the galaxy and cluster populations inside a large cosmological volume, in a Λ CDM universe. This is a challenging task: to obtain statistically

meaningful results, we need to simulate a volume sufficiently large to contain several massive clusters. At the same time, we need to describe the formation and evolution of the galaxy population down to low-mass galaxies. To achieve this, we combine a large N-body cosmological simulation with a semi-analytical subgrid treatment of galaxy formation, merging, and tidal destruction. The objectives of this work are (1) to determine if the observational results reported by Coziol et al. (2009), Skibba et al. (2011), and others can be reproduced using a numerical simulation, (2) to investigate the role played by major mergers in the build-up of clusters, and determine if the merging-group scenario constitutes a valid explanation for the observational results, and (3) to check the robustness of the various statistics used to assess the success or failure of the central galaxy paradigm.

The remainder of this paper is organized as follows. In section 2, we describe our algorithm for simulating the formation and evolution of the galaxy and cluster populations. Results are presented in Section 3. Summary and conclusion are presented in Section 4.

2. The Numerical Algorithm

The numerical algorithm is described in details in Barai et al. (2009) and Martel et al. (2012). In this paper, we reuse the simulation that was presented in Martel et al. (2012). We simulate the formation of large-scale structures in a cubic volume of comoving size 100 Mpc, using a Particle-Mesh (PM) algorithm, with 512^3 equal-mass particles and a mesh 1024^3 . The mesh spacing is 97.7 kpc, which gives the comoving length resolution of the algorithm. We assume a concordance Λ CDM model with density parameter $\Omega_0 = 0.268$, cosmological constant $\lambda_0 = 0.732$, and Hubble constant $H_0 = 70.4 \text{ km s}^{-1} \text{ Mpc}^{-1}$. The total mass in the box is $M_{\text{tot}} = 3.686 \times 10^{16} M_\odot$ and the mass per particle is $M_{\text{part}} = 2.747 \times 10^8 M_\odot$. Galaxies are represented by using one single particle per galaxy. The code creates galaxies each of mass $M_{\text{min}} = 2 \times 10^9 M_\odot$ in regions where the density exceeds 200 times the mean density of the universe at that redshift. When that condition is satisfied, a “galaxy particle” is introduced, and the masses of the nearby particles is reduced accordingly. As the simulation proceeds, these galaxy particles are allowed to merge, forming more massive galaxies at later epochs. They can also tidally disrupt one another. The mergers and tidal disruption of galaxies are modeled using a semi-analytical prescription. For details, we refer the reader to Martel et al. (2012). As we showed in that paper, this algorithm successfully reproduces the observed luminosity function of galaxies, and provides a full description of the history of galaxy and cluster formation.

The algorithm keeps track of the total mass M_{gal} of each galaxy. To facilitate comparison with observations, we ascribe a stellar mass and a luminosity to each galaxy. We calculate luminosities using the M/L ratio given in Yang et al. (2003), equation (17):

$$\left\langle \frac{M_{\text{gal}}}{L_{\text{gal}}} \right\rangle = \frac{1}{2} \left(\frac{M}{L} \right)_0 \left[\left(\frac{M_{\text{gal}}}{M_1} \right)^{-\beta} + \left(\frac{M_{\text{gal}}}{M_1} \right)^{\gamma_1} \right], \quad (1)$$

where $M_1 = 10^{11.27} h^{-1} M_\odot$, $(M/L)_0 = 134 h M_\odot / L_\odot$, $\beta = 0.77$, and $\gamma_1 = 0.32$ (this is their M1 model). We can estimate the luminosity of a galaxy using $L_{\text{gal}} = M_{\text{gal}} / \langle M_{\text{gal}} / L_{\text{gal}} \rangle$. Since $\gamma_1 < 1$, L_{gal} increases monotonically with M_{gal} . Hence, we will assume that, in each simulated cluster, the BCG is simply the most massive galaxy in the cluster. We should keep in mind that is an estimate, because $\langle M_{\text{gal}} / L_{\text{gal}} \rangle$ is an average over an ensemble of galaxies. In the real universe, there might be some clusters in which the BCG is not the most massive galaxy. To estimate the stellar mass M_* , we use the fitting formula given by Behroozi et al. (2010), equations (21) and (22). The stellar mass and luminosity corresponding to the minimum galaxy mass M_{min} are $M_{*,\text{min}} = 8.5 \times 10^4 M_\odot$ and $L_{\text{min}} = 9.5 \times 10^5 L_\odot$, respectively.

The simulation produces 50 dumps between redshifts $z = 7.7$ and $z = 0$.² Each dump contains the positions, velocities, and masses of three types of particles: the P³M particles the simulation started with, the particles representing galaxies, and the particles representing tidal fragments, that is, galaxies that have been destroyed by tides. These latter particles do not enter in the analysis, except when computing the global properties of clusters (total mass, center-of-mass position and velocity, velocity dispersion, ...).

For each dump, we build a cluster catalog, using a standard Friends-of-Friends algorithm with a linking length equal to 1/4 of the mean particle spacing (that is, 48.8 kpc comoving). All three types of particles are included. We excluded clusters containing fewer than 4000 particles, corresponding to a mass $M_{\text{cl}} \approx 1.1 \times 10^{12} M_\odot$. At $z = 0$, the simulation volume contains 1788 clusters. Two of these clusters have a mass $M_{\text{cl}} > 10^{15} M_\odot$ and 16 more clusters have a mass $M_{\text{cl}} > 10^{14} M_\odot$. This is consistent with the observed mass function of clusters (Bahcall & Cen 1993). We also calculated the radial projected density profiles of clusters, following Díaz et al. (2005). For each cluster, we first calculated the virial radius r_{200} , and then the projected surface density Σ calculated using galaxies only. We then averaged over clusters to get Σ as a function of r/r_{200} . The length resolution of our simulation is 100 kpc. In order to compute Σ over one decade in radius, from $0.1 r/r_{200}$ to $1.0 r/r_{200}$, we selected all clusters with $r_{200} \geq 1$ Mpc, thus ensuring that the entire range in radius is above the resolution limit. This represents a total of 28 clusters for the whole simulation. The results are plotted in Figure 1 (circles). The solid curve is not a fit to our own results, but rather a fit to the clusters in the 2dF survey. This fit is taken directly from the top left panel of Figure 8 in Díaz et al. (2005), using the parameters listed in their Table 2. Because we included only 28 clusters, our error bars are larger than the ones in Díaz et al. (2005), but the results are consistent.

²The actual simulation starts at redshift $z = 24$, but the first galaxies form at $z = 7.7$, so earlier dumps are not useful.

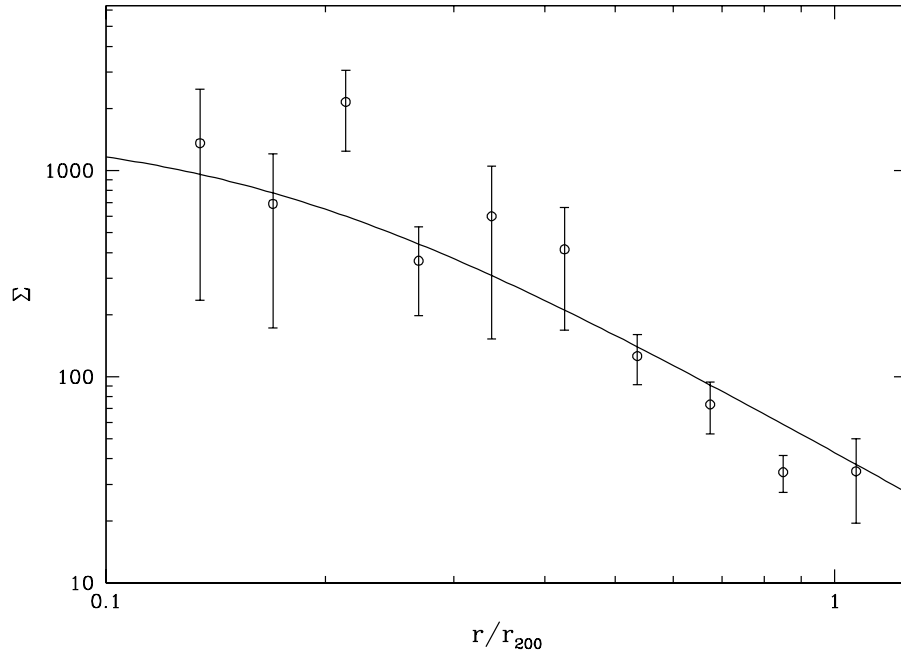


Fig. 1.— Projected galaxy surface density Σ versus r/r_{200} , averaged over all 28 clusters with $r_{200} \geq 1$ Mpc (circles). Error bars show $1\text{-}\sigma$ uncertainty on the value of the mean. The solid curve shows a fit to the clusters in the 2dF survey (see text).

3. Results

3.1. The Samples of Galaxies and Clusters

In the following subsections, we compare our results with observations, focusing on two recent observational studies: Coziol et al. (2009) and Skibba et al. (2011). Before making these comparisons, we want to mention the similarities and differences between our numerical samples and their observational ones. Skibba et al. (2011) used the SDSS galaxy group catalog of Yang et al. (2007). It contains 277 838 galaxies with magnitude $m < 17.77$ and redshift $z \leq 0.2$, forming 215 493 clusters (they use the word “group”). Hence, most clusters contain only one galaxy. From this sample, they selected for analysis a subsample of 6760 clusters with masses $M_{\text{cl}} > 10^{12} h^{-1} M_{\odot}$ containing at least 3 galaxies each. Coziol et al. (2009) selected 1169 clusters from the catalog of Abell et al. (1989). This sample includes only rich clusters up to redshift $z = 0.2$, with at least 30 galaxies in the magnitude range $[m_3, m_3 + 2]$, where m_3 is the magnitude of the third brightest member. They identified the BCG in each cluster, and retained several candidates when the identification was ambiguous, so they ended up with 1426 BCG’s. Their analysis does not involve satellite galaxies (galaxies other than the BCG’s). In our simulation, the number of galaxies increases with time. At $z = 0$ our numerical sample consists of 79 751 galaxies with mass $M_{\text{gal}} \geq 2 \times 10^9 M_{\odot}$. The Hubble velocity across the computational volume is $v = (70.4 \text{ km s}^{-1} \text{ Mpc}^{-1})(100 \text{ Mpc}) = 7400 \text{ km s}^{-1}$, corresponding to a redshift $z = 0.0235$ which can be taken as the depth of our sample. We identify 1788 clusters with a mass $M_{\text{cl}} > 1.1 \times 10^{12} M_{\odot}$. These clusters contain a total of 51 801 galaxies, with one galaxy per cluster in the poorest ones, and 7765 galaxies in the richest one (cluster C01, see section 3.5 below). Hence, our sample is similar to the one used by Coziol et al. (2009) in terms of number of clusters. Our shallower depth ($z = 0.0235$ compared to 0.2) is compensated by the fact that a numerical simulation provides an effective sky coverage of 100%. The sample used by Skibba et al. (2011) is significantly larger than ours, with 2.7 times more galaxies and 3.7 times more clusters, with the minimum cluster mass 30% lower than ours.

3.2. Location of the Brightest Cluster Galaxy (BCG)

For each cluster, we calculated the projected distances between the galaxies and the center of mass of the cluster. We only considered galaxies with total masses $M_{\text{gal}} > 10^{10} M_{\odot}$, corresponding to a stellar mass $M_{*} = 3.27 \times 10^6 M_{\odot}$ and a luminosity $L = 1.57 \times 10^7 L_{\odot}$. This is our mock detection limit. We then identify the brightest galaxy, and the galaxy closest to the center. Figure 2 shows the fraction f_{BNC} of clusters in which the brightest galaxy is not the central one, versus the mass of the clusters. We average over bins of width $\Delta(\log M_{\text{cluster}}) = 0.5$. Error bars are $1\text{-}\sigma$ uncertainties on the value of the mean for each bin, that is, the standard deviation divided by the square root of the number of clusters in each bin (we refer the reader to Skibba et al. 2011 for the calculation of the horizontal error bars on their results). The solid circles show the results for our simulated clusters, at $z = 0$. The solid triangles, open triangles, and open squares are taken directly from

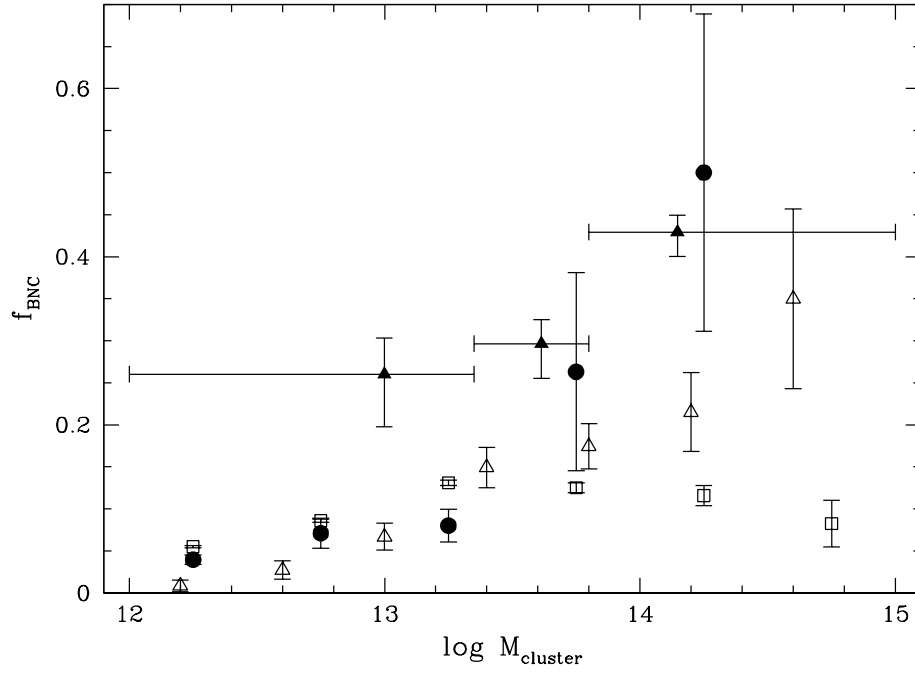


Fig. 2.— Fraction of clusters at $z = 0$ in which the brightest galaxy is not the one closest to the center, versus cluster mass. Solid circles: our results at $z = 0$; solid triangles: results of Skibba et al. (2011); open triangles: predictions from the MORGANA semi-analytic model; open squares: predictions of Croton et al. (2006) semi-analytic model.

Figure 9 of Skibba et al. (2011). The solid triangles show their results, while the open symbols show the predictions of the MORGANA semi-analytical model (Monaco et al. 2007; Lo Faro et al. 2009, open triangles) the semi-analytical model of Croton et al. (2006) (open squares).

We find that f_{BNC} increases with cluster mass. This is consistent with the results of Skibba et al. (2011) and of the MORGANA model, while the Croton et al. (2006) model predicts a drop in f_{BNC} at masses $M_{\text{cluster}} > 10^{13} M_{\odot}$. In this mass range, our results are, within error bars, fully consistent with the ones of Skibba et al. (2011). At lower masses, our simulations and the semi-analytical models all predict that f_{BNC} continues to decrease with decreasing cluster mass, while the results of Skibba et al. (2011) show levelling-off of f_{BNC} around 0.25 at low masses. These authors speculate that the discrepancy between the observational results and the predictions of the semi-analytical models is caused by various shortcomings of the latter. In particular, the dynamical friction time-scale tends to be too short in semi-analytical models, resulting in galaxies being accreted too rapidly. We do observe a similar phenomenon at the late stages of our simulation, as discussed in Martel et al. (2012). Adding this to the fact that our simulation does not include galaxies with masses below $M_{\text{min}} = 2 \times 10^9 M_{\odot}$, we probably have a deficit of low-mass galaxies in small clusters, which would explain the low values of f_{BNC} . For this reason, we will avoid drawing any conclusion based on the value of f_{BNC} for low-mass clusters.

Figure 3 shows f_{BNC} vs. cluster mass at three different redshifts, $z = 0.5$, 0.2 , and 0 , for our simulation. The corresponding lookback times (time elapsed since those redshifts) are $t = 5.07$ Gyr, $t = 2.43$ Gyr, $t = 0$ Gyr, respectively. Within error bars, f_{BNC} is independent of redshift. Ideally, clusters should evolve toward equilibrium with time. The fact that f_{BNC} does not decrease with time implies that some process is maintaining clusters out of equilibrium. Major and semi-major mergers are the likely culprits, as we shall see later.

3.3. Resolution, Projection, and Selection Effects

The resolution limit of our simulation is of order 100 kpc. This might cause a problem if several galaxies, including the BCG, are located within that distance to the center. In such case, we could not unambiguously determine which galaxy is the closest to the center. Fortunately, a central region of radius 100 kpc is quite compact, and the likelihood of finding several galaxies in that region is small. We counted the number of galaxies in the central region at $z = 0$ for all 1788 clusters in the simulation. We found 465 clusters with no galaxy in the central region, 1312 clusters with one galaxy, 11 clusters with two galaxies, and no cluster with more than two galaxies. Hence, there is an ambiguity in identifying the central galaxy for 11 clusters, or 0.6% of the cluster population. Furthermore, all these are low-mass clusters. The most massive has a mass of $3.3 \times 10^{13} M_{\odot}$ and the 10 others have a mass below $10^{13} M_{\odot}$. As we explained above, we are avoiding drawing conclusions based on the value of f_{BNC} for these clusters.

There are two other sources of uncertainties in the determination of f_{BNC} for a given redshift

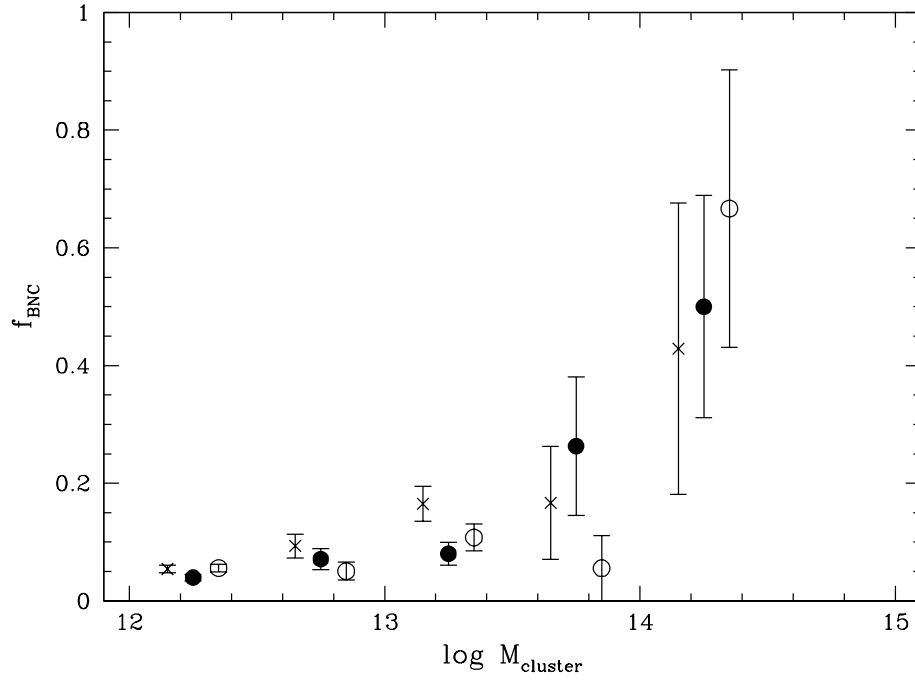


Fig. 3.— Fraction of clusters in which the brightest galaxy is not the one closest to the center, versus cluster mass, in our simulation. The various symbols show the results at $z = 0$ (solid circles), $z = 0.2$ (open circles), and $z = 0.5$ (crosses). For clarity, results at $z = 0.2$ and $z = 0.5$ were shifted by $\log M_{\text{cluster}} = +0.1$ and -0.1 , respectively.

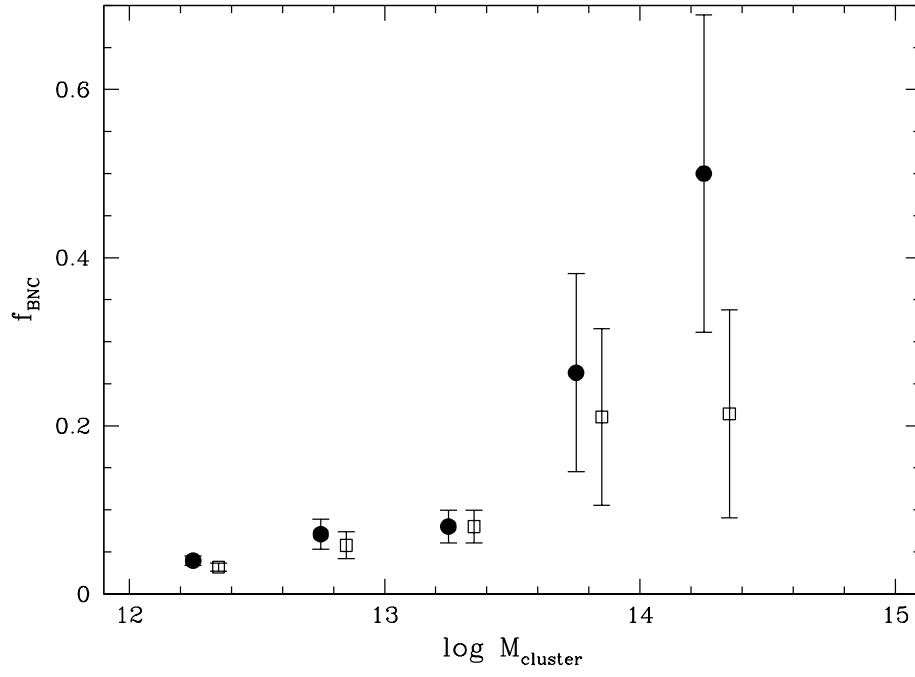


Fig. 4.— Fraction of clusters at $z = 0$ in which the brightest galaxy is not the one closest to the center, versus cluster mass, in our simulation. Solid circles: f_{BNC} calculated using projected distances, as in Figures 2 and 3; open squares: f_{BNC} calculated using actual 3D distances. For clarity, the latter results were shifted by $\log M_{\text{cluster}} = +0.1$.

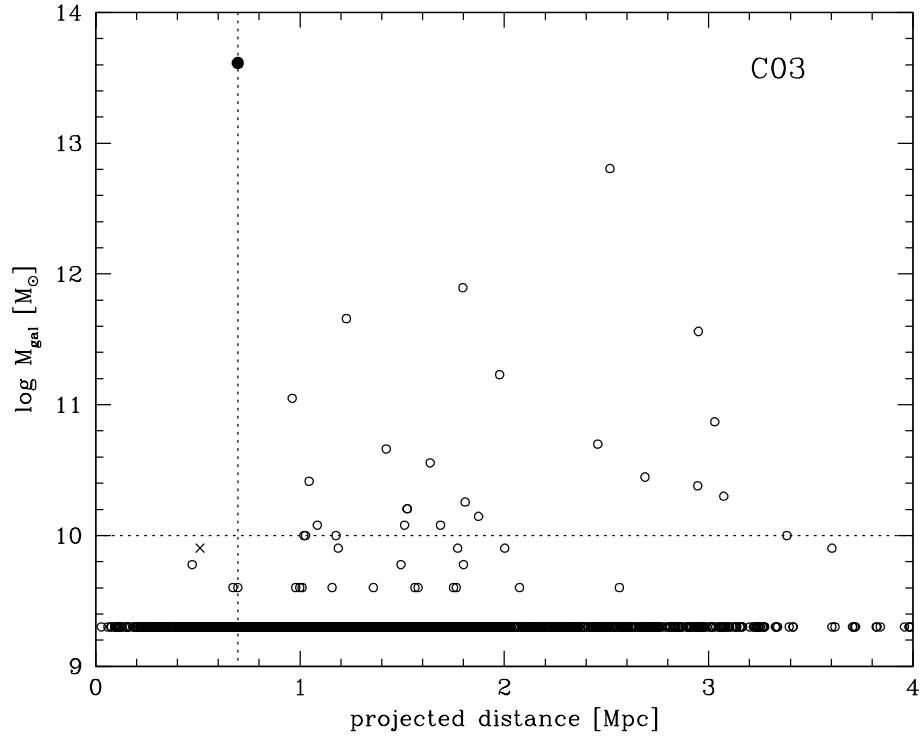


Fig. 5.— Masses and projected distances to the center of all galaxies belonging to cluster C03 (see section 3.5). The solid circle identifies the BCG. The cross identifies a galaxy whose mass is just below the detection threshold $M_{\text{gal}} = 10^{10} M_{\odot}$.

and mass range. The first one is statistical. f_{BNC} is the fraction of clusters for which the BCG is not the closest galaxy to the center. The more clusters we have, the more accurate the determination of f_{BNC} will be. This is illustrated by the error bars in Figures 2 and 3. These error bars become very large at high masses because we only have a few clusters in these mass bins. The second source of uncertainty comes from the difficulty in determining whether, for a particular cluster, the BCG is the closest galaxy to the center or not. Two effects make this determination difficult. First, observers deal with projected distances on the plane of the sky, whereas the distance that enters in the central galaxy paradigm is actually the 3D distance. In a simulation, we have the luxury of knowing all components of the positions, and we can therefore calculate 3D distances. So we recalculated f_{BNC} , using this time the full 3D separation between the galaxies and the center of mass of the clusters. In Figure 4, we compare these results with the ones obtained using the projected distances. At low masses, the results are nearly identical, or well within error bars. Things are different in the highest mass bin: the “real” value f_{BNC} , the one computed using 3D distances, appears to be significantly below the “observed” value which is computed using projected distances, in spite of the large error bars. A false positive might be recorded when a galaxy that is not the BCG appears to be close to the center, but is merely aligned with it. These projection effects should become more common as the number of galaxies increases, which explains why this problem is found only in high-mass clusters. However, the same problem should appear in lower-mass bins if the detection limit of galaxies is shifted to lower luminosities.

This brings us to the second effect. The total number of galaxies observed in each cluster will depend on the detection limit. If this limit is lower, more galaxies will be detected, and the odds that one of them will be closer to the center than the BCG (either in 3D or in projection) will increase. For this reason, any value of f_{BNC} determined from observations should be taken as a lower limit, owing to the fact that we might be missing faint galaxies located near the center. To illustrate this, we focus on one particular cluster in our simulation, cluster C03. This is the third most massive cluster in our simulation, with a total mass $M_{\text{cl}} = 5.62 \times 10^{14} M_{\odot}$. Figure 5 shows the masses and projected distances to the center for all galaxies in the cluster.³ The solid circle and the vertical line indicate the BCG and its projected distance to the center, respectively. The horizontal dotted line indicates the detection limit we used to determine f_{BNC} . Above that line, all galaxies are located at distances larger than the BCG, hence this cluster is identified as one for which the BCG is the closest to the center, and therefore this cluster does not contribute to the value of f_{BNC} . But if the detection limit is slightly lowered, then a low-mass galaxy, indicated by a cross, suddenly becomes visible, and the BCG is no longer the closest galaxy to the center. This could explain the discrepancy between our values of f_{BNC} and the ones reported by Skibba et al. (2011), if their low-mass clusters contain large numbers of low-mass galaxies, but this is unlikely since most of the clusters in their sample contain 5 galaxies or fewer (see their Figure 1).

³We remind the reader that, in our simulation, all galaxy masses are multiples of $M_{\text{min}} = 2 \times 10^9 M_{\odot}$, which explains the horizontal alignment seen in the bottom of the figure.

Finally, there is a third effect: the uncertainty in determining the location of the center. This location is always approximate, whether it is determined from observations or from a simulation. Observations are limited by projection effects, detection limits, poor sampling (having too few observed galaxies in the cluster), or in the case of dynamical estimates, only having the radial component of the velocities. Simulations have their own problems: clusters do not have sharp edges, and tend to blend into filaments and larger structures. An algorithm for identifying clusters, like the friends-of-friends algorithm, must use a particular value for the linking length, and it is this particular value which sets, somehow arbitrarily, the edges of the clusters. For these reasons, we can never be sure which galaxy is the closest to the center if the differences in distances are very small. We actually use this limitation to justify the resolution of our simulation. The *physical* length resolution is of order 40 kpc at $z = 1.5$ and 100 kpc at $z = 0$. We do not think that the location of clusters's centers could be determined with a precision better than that. Also, the location of the center depends on the method used for estimating it. We use the center of mass of the cluster, but we also tried using the galaxies only, as in Skibba et al. (2011). For high-mass clusters, the differences were of order the resolution length of the algorithm or less; for low-mass clusters, the number of galaxies was too small to allow a reliable determination of the center.

3.4. Velocity of the Brightest Cluster Galaxy

According to the central galaxy paradigm, the BCG should be at rest relative to the cluster. Following Coziol et al. (2009), we calculate the difference in radial velocity between the BCG and the cluster itself. We assume that the observer is located in the $-z$ direction, at a distance significantly larger than the size of the cluster. Hence, the z -component can be taken as the radial component. The velocity difference is then given by

$$\Delta v = |v_{\text{BCG},z} - v_{\text{cl},z}|. \quad (2)$$

Using this, we calculate the ratio $\Delta v/\sigma$, where σ is the 1D velocity dispersion. $v_{\text{cl},z}$ and σ are calculated using

$$m_{\text{tot}} = \sum_{i=1}^N m_i, \quad (3)$$

$$v_{\text{cl},z} = \frac{1}{m_{\text{tot}}} \sum_{i=1}^N m_i v_{i,z}, \quad (4)$$

$$\sigma^2 = \frac{1}{N} \sum_{i=1}^N (v_{i,z} - v_{\text{cl},z})^2. \quad (5)$$

where m_i and $v_{i,z}$ are the mass and the z -component of the velocity of particle i . Two different approaches can be used to estimate $v_{\text{cl},z}$ and σ for a given cluster: We can include only the galaxy

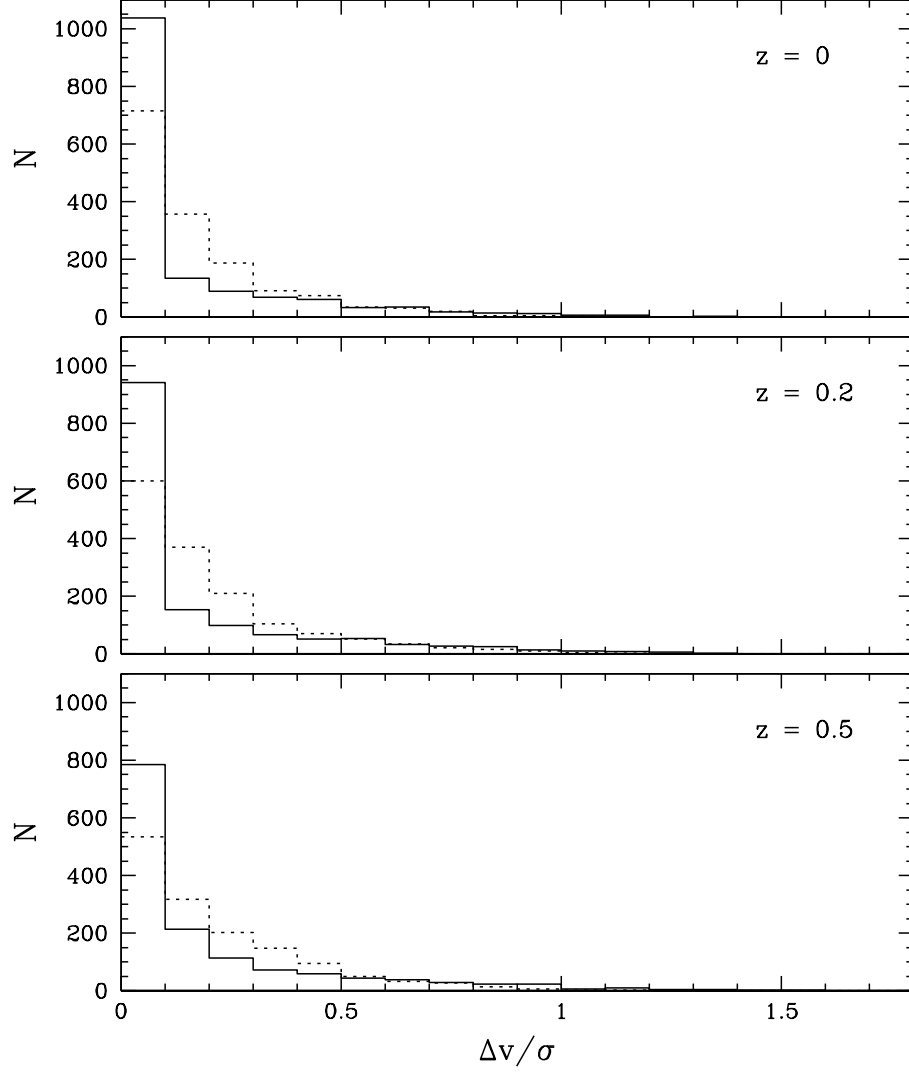


Fig. 6.— Distributions of values of $\Delta v / \sigma$ for all clusters. Solid lines: $\sigma = \sigma_{\text{gal}}$; dotted lines: $\sigma = \sigma_{\text{matter}}$;

particles in the sums. This corresponds to what an observer would do. Or we can use all particles: galaxies, dark matter, and tidal fragments. Here we use both approaches.

Figure 6 shows the distribution of values of $\Delta v/\sigma$ at three different redshifts, calculated using the galaxies (solid lines), and using all the matter in the cluster (dotted lines) to calculate $v_{\text{cl},z}$ and σ . The distributions are very skewed toward low values, and do not show much dependence on redshift. There is a shift toward higher values when all the mass in clusters is used for the calculation. Comparing this figure with Figure 2 of Coziol et al. (2009), we find some interesting similarities. In particular, our largest values of $\Delta v/\sigma$ are of order 1.8, which is fully consistent with their results. However, their distributions are much less skewed than ours. This is reflected in the medium values of $\Delta v/\sigma$. Coziol et al. (2009) found a median value of 0.32. Our values are listed in Table 1. Our median values are in the range 0.03–0.08 when using the galaxies only, and raise to 0.15 when using the whole cluster. The difference between our results and theirs could be a selection effect since their sample is limited to massive, Abell-like clusters. We recalculated the distribution of $\Delta v/\sigma$, this time using only the 18 clusters in our simulation that have a mass $M_{\text{cl}} > 10^{14} M_{\odot}$. The results are shown in Figure 7. The distributions are much wider than the ones shown in Figure 6, and also, within the noise, there are no significant difference between the two histograms. The median values are now in the range 0.15–0.28 when using galaxies (Table 1) which is more consistent with the results of Coziol et al. (2009). As we argued in the previous section, we expect low-mass clusters at $z = 0$ to be closer to equilibrium than higher-mass ones. Then we would naturally expect the distribution of $\Delta v/\sigma$ to get skewed toward lower values as lower-mass clusters are included in the sample.

3.5. The History of the Massive Clusters

All massive clusters form by the hierarchical mergers of smaller clusters. We characterize mergers as *major*, *semi-major*, and *minor*, depending on the mass ratio between the two most massive progenitors. A merger is considered major if the mass ratio is less than two (for instance,

Table 1. Median values of $\Delta v/\sigma$.

z	$(\Delta v/\sigma_{\text{gal}})_{\text{med}}$	$(\Delta v/\sigma_{\text{matter}})_{\text{med}}$
All clusters		
0.0	0.033	0.107
0.2	0.047	0.129
0.5	0.076	0.149
$M_{\text{cl}} > 10^{14} M_{\odot}$ clusters		
0.0	0.150	0.118
0.2	0.156	0.151
0.5	0.277	0.313

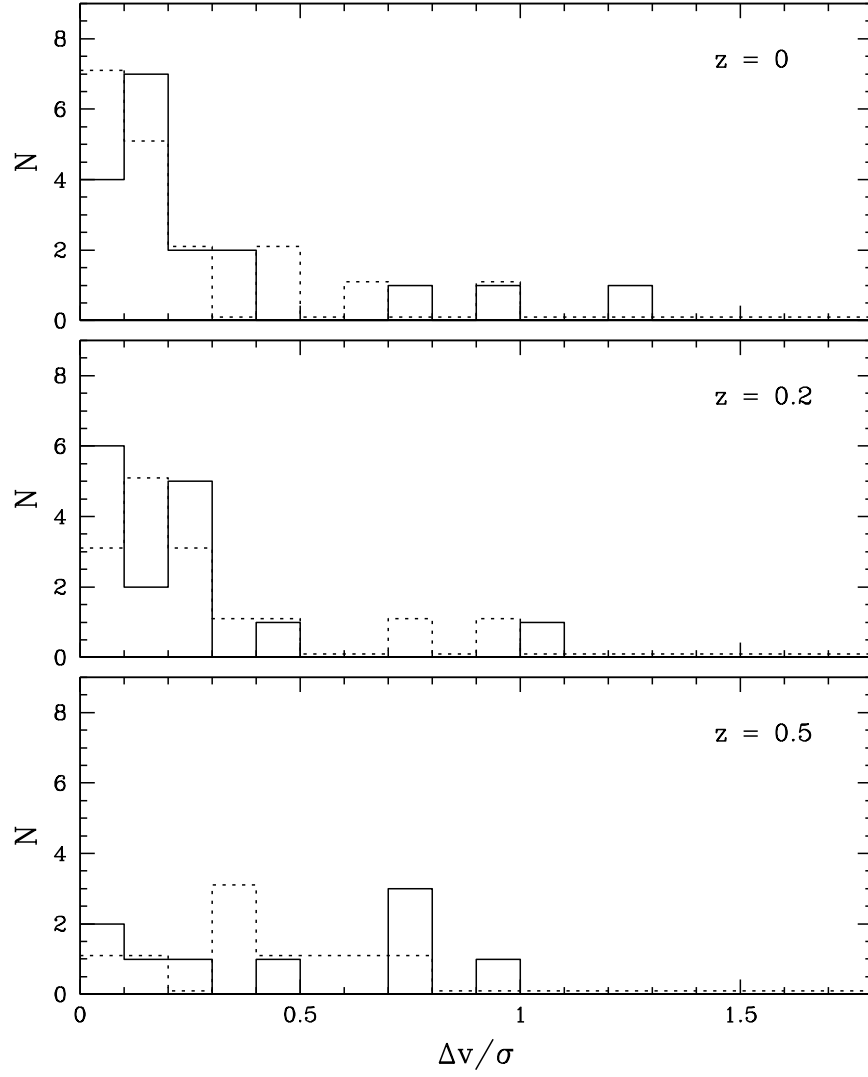


Fig. 7.— Same as Fig. 6, for all 18 clusters with mass $M_{\text{cl}} > 10^{14} M_{\odot}$.

a 56/38 merger or a 44/31/18 merger, where the numbers indicate the percentage of final mass contributed by the main progenitors). It is considered semi-major if the mass ratio is between two and four (for instance, a 68/21 merger), and minor if the ratio exceeds four (for instance, a 82/13 merger). Semi-major mergers are mergers in which one progenitor dominates, but the second most massive progenitor does provide an important contribution.

Using all 50 cluster catalogs between $z = 7.7$ and $z = 0$, we built the merger trees of all 18 clusters with masses $M > 10^{14} M_{\odot}$. For each tree, we identified the “main family line” of the cluster. To do so, we start with the root of the tree at $z = 0$, and move backward in time. When we encounter a merger, we follow the path of the most massive progenitor. For each cluster along the main family line, we calculated the projected physical distance, from the center of mass of the cluster, of the brightest galaxy and the nearest galaxy. These distances are shown as circles and crosses in Figure 8. Often the two symbols coincide, indicating that the brightest galaxy is indeed the nearest to the center. This is the case at all redshifts for clusters C08 and C16. In other cases, the difference in distances between the brightest and most central galaxies can be large, especially in the most massive clusters like C01, C02, C04, C05, and C07. Notice that the accuracy in the determination of the distances depends on the finite resolution of the code. The comoving resolution is 100 kpc. The physical resolution is therefore 100 kpc at $z = 0$, and 40 kpc at $z = 1.5$. This corresponds to the first small tick on the right-hand side of each panel in Figure 8, and 2/5 of that on the left-hand-side. When several galaxies are that close to the center, we cannot be sure which one is the BCG. But fortunately, with these clusters containing between 9 and 53 galaxies, there are rarely more than one galaxy that close to the center at a given time.

To illustrate what happens during the evolution of a cluster, we focus on cluster C04. Figure 8 shows that a dramatic event takes place around $z = 0.55$ when the most massive galaxy goes from being located 200 kpc away from the center, and being the closest galaxy to the center, to being located 2.2 Mpc away from the center. Examination of the merger tree for that cluster reveals that a major merger took place at $z = 0.56$, with three progenitors providing respectively 45%, 32%, and 17% of the total mass of the merger remnant. Figure 9 shows the evolution of cluster C04, starting at $z = 0$ and moving back in time along the main family line. In each panel, we show the brightest galaxy (green dot), and all other galaxies more massive than $10^{10} M_{\odot}$ (yellow dots). Notice that if we had plotted all galaxies down to the resolution limit $2 \times 10^9 M_{\odot}$ of the simulation, each panel would have between 1000 and 1800 galaxies. The magenta cross indicates the location of the center of mass.

In the top left panel, we plotted the two largest progenitors that are about to undergo a major merger with the main progenitor. The contribution of each progenitor in percentage is indicated. We used yellow dots to identify the galaxies belonging to the main progenitor, and orange and red dots to identify the ones belonging to the other progenitors. The three clusters appear to be in contact already, but this is a projection effect. The actual merger takes place at $z = 0.56$. We actually see four mass concentrations on this panel: a central one, a left one, a lower one, and an upper right one. The central and lower concentrations are actually parts of a same cluster. This

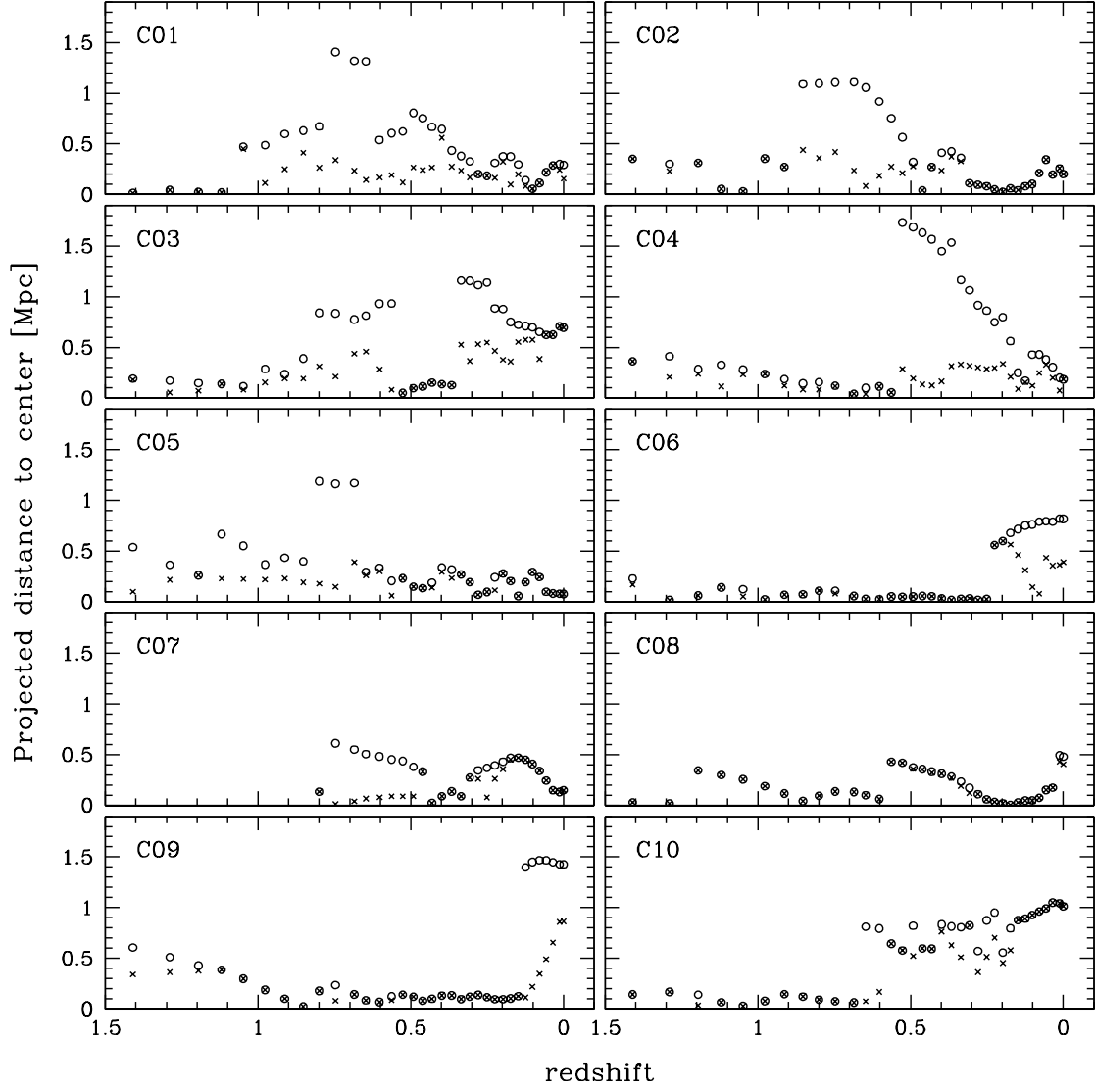


Fig. 8.— Distance to the center of the brightest galaxy (open circles) and the galaxy nearest to the center (crosses), versus redshift, for each merger tree, as indicated. The length resolution varies linearly from 40 kpc at $z = 1.5$ to 100 kpc at $z = 0$.

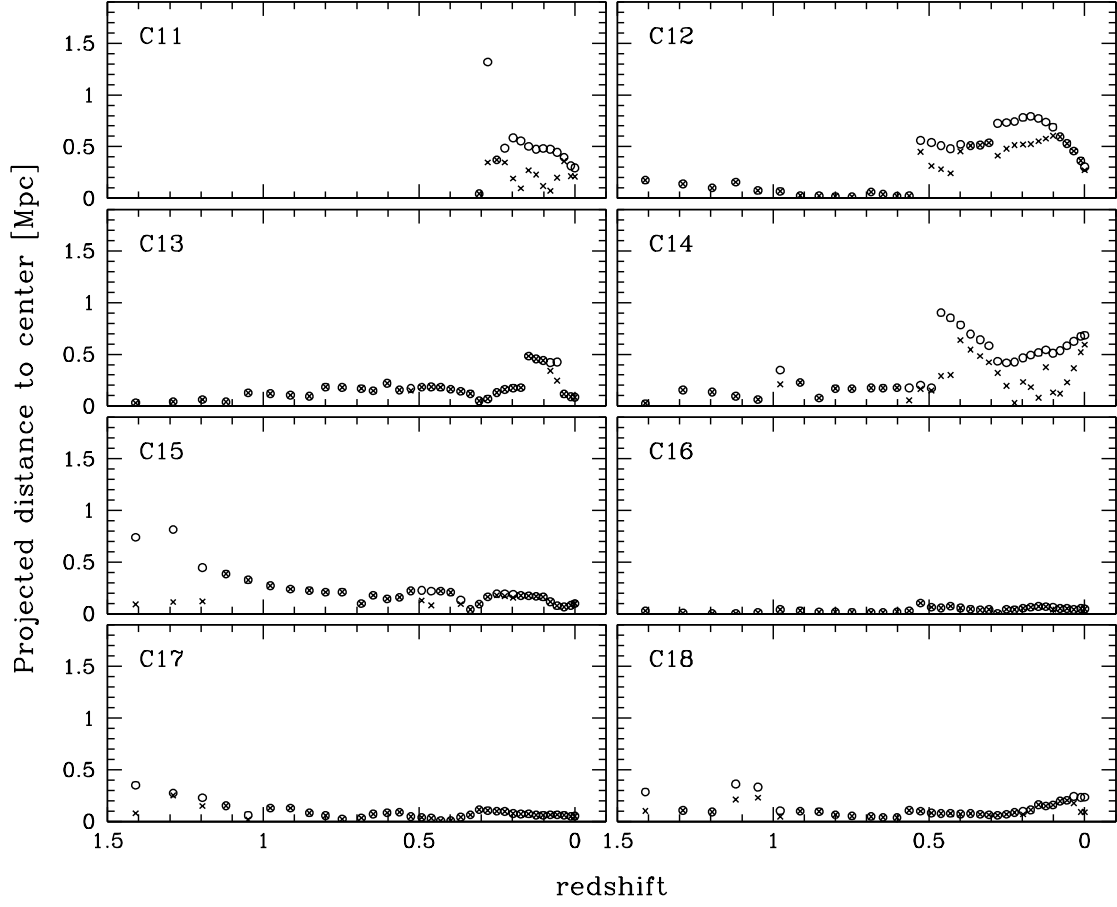


Fig. 8.— continued.

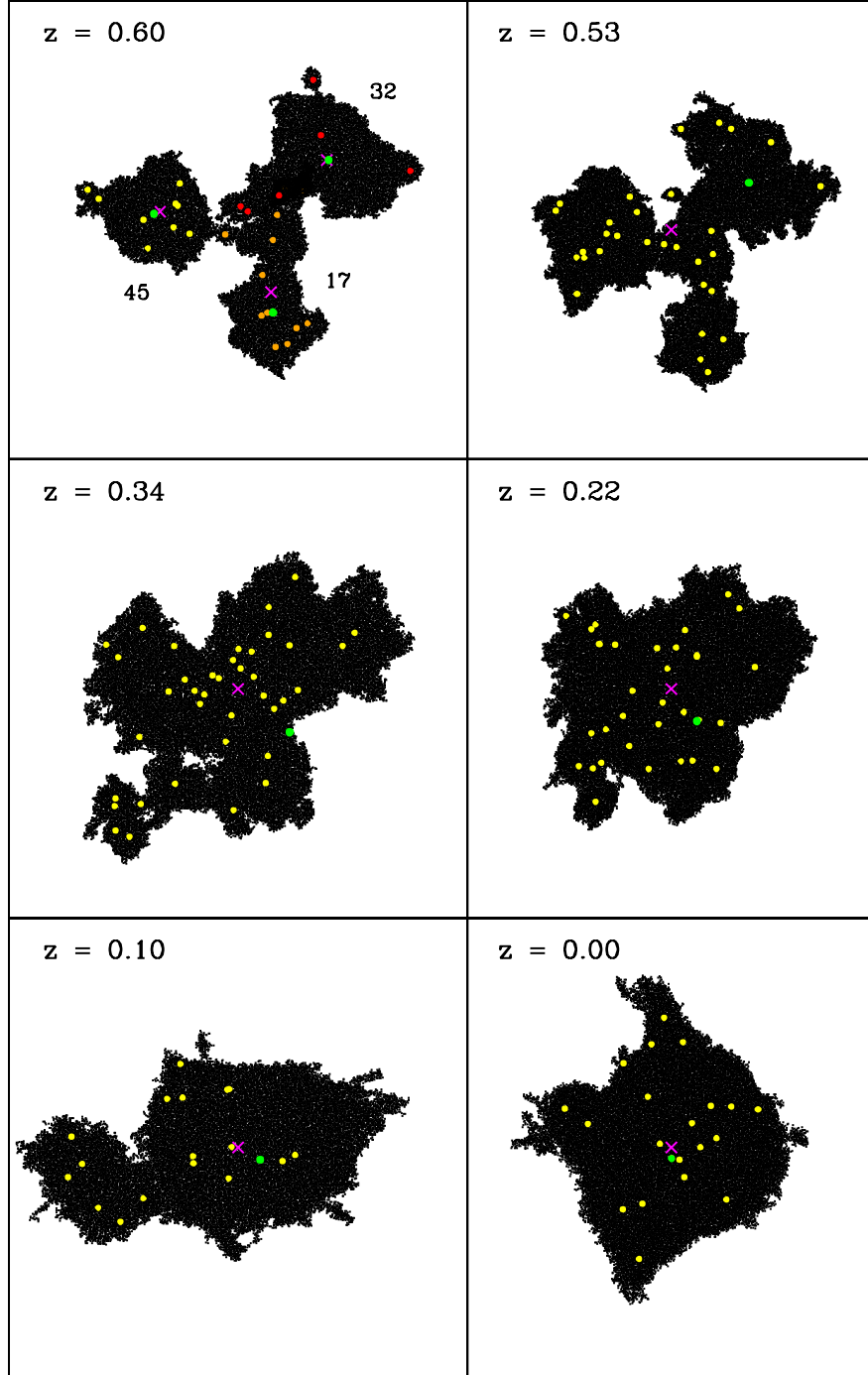


Fig. 9.— Evolution of cluster C04 along the main family line. Each panel shows the cluster at a particular redshift, as indicated. Black area: dark matter; green dot: brightest galaxy; yellow dots: other galaxies more massive than $10^{10} M_{\odot}$; magenta cross: position of the center of mass. Top left panel shows two additional clusters plotted together with the main one, with galaxies represented with orange and red dots, respectively. Numbers in top left panel indicate, in percentages, the contribution of each progenitor to upcoming major merger. Each panel is $8 \text{ Mpc} \times 8 \text{ Mpc}$ in size (proper, not comoving). The length resolution corresponds to about $1/3$ of the width of the magenta cross at $z = 0.00$, and $1/5$ at $z = 0.60$.

is the result of a semi-major merger that took place earlier at $z = 0.64$, with the central and lower parts contributing respectively 65% and 25% of the mass of the cluster. We indicated, for each cluster, the location of the brightest galaxy (green dot) and the center of mass (magenta cross). In the main progenitor, on the left, the brightest galaxy is located near the center of the cluster, and is closer than any other galaxy in the cluster. This is also the case for the upper right progenitor. But for the lower progenitor, there is a definite offset, a result of the recent merger at $z = 0.64$.

At $z = 0.53$, the three progenitors have merged to form a single cluster, with its own brightest galaxy and center of mass (top right panel). Interestingly, the brightest galaxy was not at the center of the main progenitor, but instead at the center of the upper right progenitor. The brightest galaxy is now located at 2.2 Mpc from the new center of mass, simply because the center of mass of the merged cluster is located about 2 Mpc away from the center of mass of the upper-right progenitor. However, the cluster is completely out of equilibrium. Between $z = 0.53$ and $z = 0$, the cluster slowly evolves toward equilibrium, as it only experiences minor mergers, the “least-minor” being a 78%–17% merger at $z = 0.36$. The brightest galaxy slowly migrates toward the center of the cluster, and by $z = 0$, when the cluster has reached equilibrium, that galaxy is again the closest to the center.

We performed the same exercise for all 18 major clusters. By examining Figure 8 we identified sudden changes in the distances. We then examined the corresponding merger trees to determine the cause of these changes. This is summarized in Table 2. The most common event is a sudden increase in the distance between the brightest galaxy and the center. It happens for all clusters except C16, and, in all cases, it immediately follows a major or occasionally a semi-major merger, except for cluster C13, where it follows a minor merger.

If major and semi-major mergers are responsible for having the BCG at large distances from the center, we expect the timing of these mergers to play a key role in determining whether the BCG can return to the equilibrium, central position before $z = 0$. In Figure 10, we plot for each cluster, the redshift when the last major merger or semi-major merger occurred (excluding clusters C13 and C16, which experienced no such merger). In all cases but three, the BCG has returned to the center of the cluster by $z = 0$. For clusters C06, C09, and C11, another galaxy is closer to the center at $z = 0$ (notice that we are now talking about *physical*, 3D distances, not projected distances). All three clusters experienced a recent major merger, at redshifts 0.25, 0.15, and 0.31, respectively, giving them little time to return to equilibrium by $z = 0$. Cluster C18 is an exception: it experienced a late semi-major merger, but was still able to reach equilibrium by the present, and therefore its BCG is closest to the center.

In Figure 11, we plot the evolution of $\Delta v/\sigma$, for all 18 clusters, calculated using the galaxies only (open circles) and the entire content of clusters (filled circles) for the calculation of $v_{z,cl}$ and σ . It is interesting to notice that both methods tend to give similar results. A case in point is cluster C14, for which the variations in $\Delta v/\sigma$ with redshift are perfectly in phase. Comparing this figure with the open circles in Figure 8, we find in several cases an *anticorrelation*: $\Delta v/\sigma$ increases

Table 2. Main Events in Evolution of Massive Clusters

Cluster	z	Event	Closest	Explanation	Ratios
C01	1.12	BCG moves away from center	No	Major merger	55/36
C01	0.85	BCG moves away from center	No	Major merger	51/41
C01	0.65	BCG moves to center	No	Major merger	37/32/24
C01	0.60	BCG moves away from center	No	Unclear	—
C02	0.91	BCG moves away from center	No	Major merger	55/38
C03	0.85	BCG moves away from center	No	Major merger	55/36
C03	0.37	BCG moves away from center	No	Semi-major merger	72/23
C04	0.56	BCG moves away from center	No	Major merger	45/32/17
C05	1.29	BCG moves away from center	No	Major merger	55/30
C05	1.19	BCG moves away from center	Yes	Semi-major merger	65/27
C05	0.85	BCG moves away from center	No	Semi-major merger	65/29
C06	0.25	BCG moves away from center	No	Semi-major merger	73/22
C07	0.80	BCG moves away from center	No	Major merger	47/46
C07	0.46	BCG becomes closest to center	Yes	Minor merger	84/11
C08	1.29	BCG moves away from center	Yes	Major merger	55/32
C08	0.60	BCG moves away from center	Yes	Semi-major merger	64/28
C09	0.15	BCG moves away from center	No	Major merger	55/40
C10	0.69	BCG moves away from center	Yes	Major merger	59/32
C10	0.60	BCG becomes closest to center	Yes	Major merger	57/36
C10	0.53	BCG moves away from center	No	Major merger	58/37
C11	0.31	BCG moves away from center	No	Major merger	48/46
C12	0.56	BCG moves away from center	Yes	Major merger	55/39
C12	0.43	BCG moves away from center	No	Major merger	48/46
C13	0.17	BCG moves away from center	Yes	Minor merger	77/19
C14	1.05	BCG moves away from center	Yes	Major merger	52/30
C14	0.85	BCG moves away from center	Yes	Major merger	61/32
C14	0.49	BCG moves away from center	No	Major merger	58/30
C15	1.55	BCG moves away from center	No	Major merger	53/36
C17	1.55	BCG moves away from center	No	Major merger	53/36
C18	1.19	BCG moves away from center	No	Semi-major merger	63/29
C18	0.17	BCG moves away from center	No	Semi-major merger	72/22

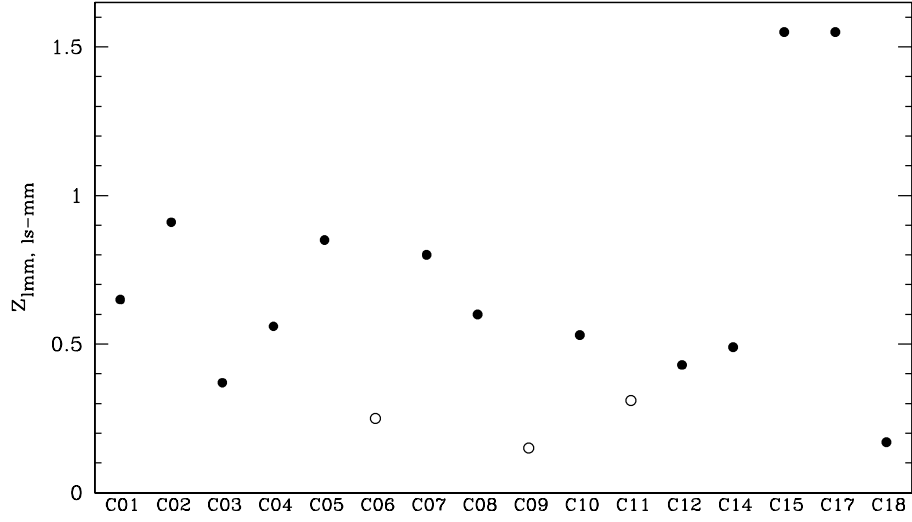


Fig. 10.— Redshift when the last major or semi-major merger occurred, for all clusters for which such a merger did occur (all but C13 and C16). Solid circles: clusters for which the BCG is the closest to the center of the cluster at $z = 0$. Open circles: clusters for which the BCG is *not* the closest to the center of the cluster at $z = 0$. These are actual 3D distances, not projected distances.

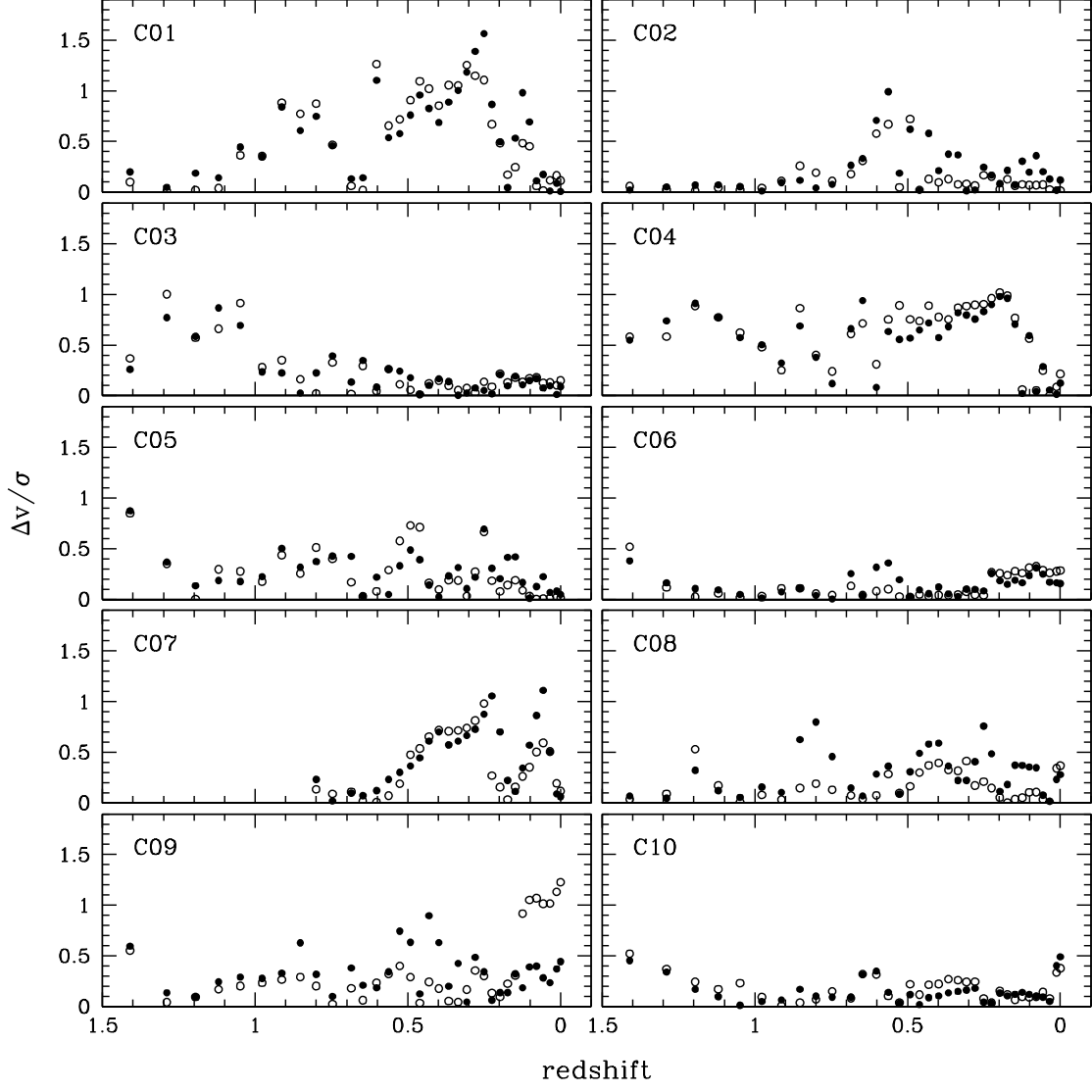


Fig. 11.— $\Delta v / \sigma$ versus redshift, for all merger trees. Filled circles: $\sigma = \sigma_{\text{matter}}$; open circles: $\sigma = \sigma_{\text{gal}}$;

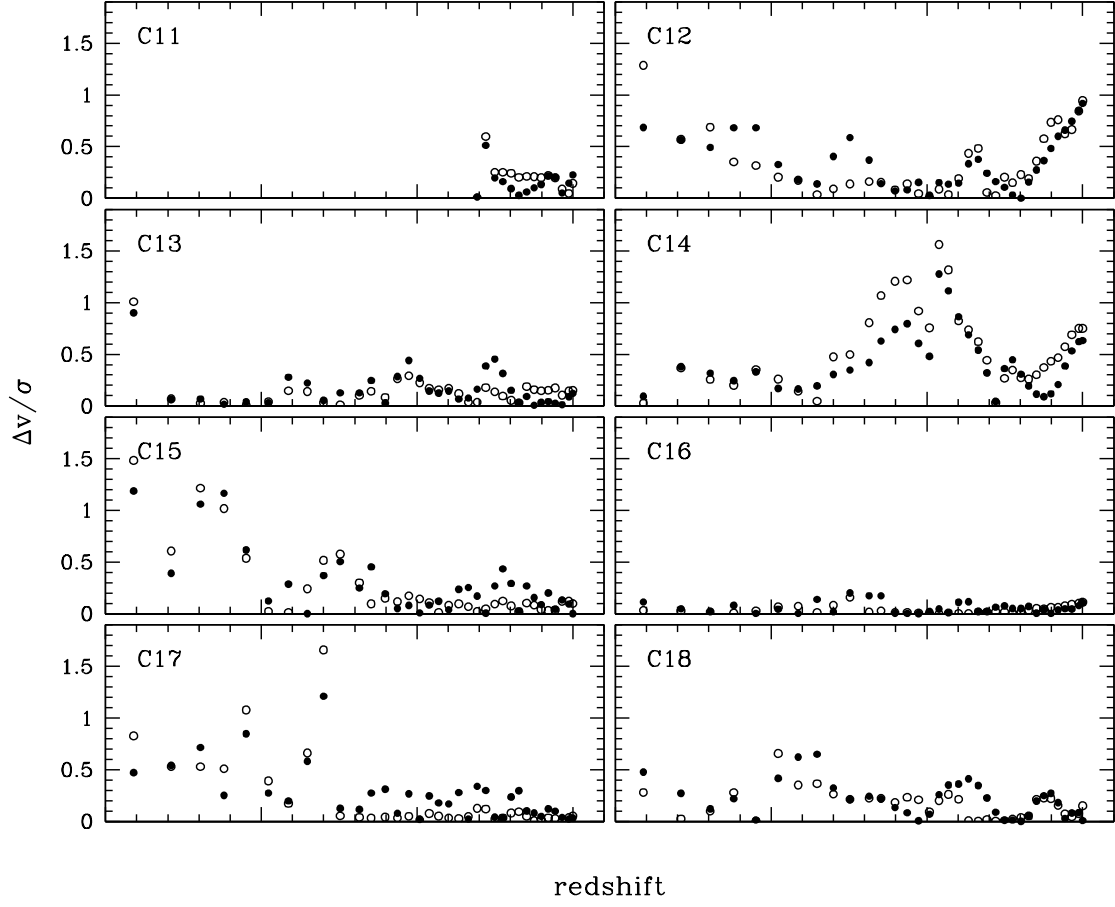


Fig. 11.— continued.

when the projected distance to the center decreases, and vice-versa. The most spectacular case is cluster C12 at $z < 0.2$, but notice also cluster C01 between $z = 0.7$ and $z = 0.3$, cluster C04 between $z = 0.6$ and $z = 0.2$, and several others. This anticorrelation could be a signature of non-equilibrium. If the BCG is moving back and forth inside the cluster, then the velocity is maximum when the BCG goes through the equilibrium position, and minimum when the BCG is the farthest from the equilibrium position (like an oscillating pendulum). Notice that we are comparing radial velocities with projected distances. Hence, this explanation is appropriate for a back-and-forth motion, but would not be appropriate for an orbital motion.

4. Summary and Conclusion

Using a cosmological N-body simulation combined with a sub-grid treatment of galaxy formation, merging, and tidal destruction, we simulated the evolution of the galaxy and cluster population in a comoving volume of size 100 Mpc, in a Λ CDM universe. In the final state of the simulation, at $z = 0$, we identified 1788 clusters, including 18 massive ones ($M_{\text{cl}} > 10^{14} M_{\odot}$). We then investigated the location and velocity of the BCG in each cluster, in order to test the validity of the central galaxy paradigm.

The fraction f_{BNC} of clusters for which the BCG is not the closest galaxy to the center increases with cluster mass. The same trend is seen in the results of Skibba et al. (2011) and in the prediction of the semi-analytical models. Furthermore, our results, within error bars, match the results of Skibba et al. (2011) at the high-mass end. However, at the low-mass end, our results predict that f_{BNC} decreases, in agreement with the semi-analytical models, but not with the results of Skibba et al. (2011), which predict a plateau at $f_{\text{BNC}} \sim 0.25$. We agree with the general conclusion of Skibba et al. (2011) that many BCGs do not reside at the center of their host cluster. However, we found that f_{BNC} is not a very robust statistics. Its determination is affected by projection effects, which may lead to an overestimate of f_{BNC} , and selection effects, which may lead to an underestimate of f_{BNC} . Uncertainties in the determination of the center of the clusters can also be a problem.

We also calculated the ratio $\Delta v/\sigma$. This is a more robust statistics, since it is not affected by projection effects, and weakly affected by selection effects through the estimation of σ . The distributions of $\Delta v/\sigma$ extend from 0 to 1.8, and are very skewed toward low values. The median values of $\Delta v/\sigma$ are in the range 0.03–0.08, significantly lower than the value 0.32 reported by Coziol et al. (2009). However, when we consider only clusters with masses $M > 10^{14} M_{\odot}$, the distributions become wider, and the median values raise to 0.15 at $z = 0$ and 0.28 at $z = 0.5$. This indicates that low-mass clusters and nearby clusters, are more likely to be in equilibrium than high-mass ones or distant ones.

We selected the 18 most massive clusters in our simulation, with masses $M > 10^{14} M_{\odot}$, and performed a detailed study of the history of their formation, focussing on the period $z = 1.5$ to

$z = 0$ (that is, the last 9.4 Gyrs). For each cluster, we built a merger tree, and followed the location and velocity of the BCG along the main family line of each cluster. A general pattern emerges. The brightest galaxy is initially the closest to the center of the cluster, and remains the closest until the cluster experiences a major or semi-major merger with another cluster of comparable mass. Immediately after that merger, the brightest galaxy can find itself at one Mpc or even more from the center of the new cluster, and in this case is no longer the closest to the center. However, the new cluster, immediately after the merger, is out of equilibrium. During the time it takes for the cluster to reach equilibrium, the brightest galaxy migrates toward the center, until it finds itself the closest to the center again.

The whole situation can be described in terms of two sets of timescales. First, we have the timescale for the clusters to form by the merger of smaller progenitors, versus the timescale for galaxies to form inside these progenitors. If the former timescale is the shorter one, which is the basic assumption behind the central galaxy paradigm, then the galaxies will form inside a system in equilibrium, and the BCG will settle at rest at the center of the cluster. But if the latter timescale is the shorter one, the galaxy destined to become the BCG is already present in one of the progenitor. The second set of timescales then comes into play: the timescale for the cluster to reach equilibrium after a major or semi-major merger, versus the timescale between such mergers. If the former timescale is the shorter one, then the cluster will reach equilibrium at $z = 0$, after the last merger. But if the latter timescale is the shorter one, then the cluster will be constantly disturbed by mergers, will never have sufficient time to reach equilibrium, and therefore will still be out of equilibrium at $z = 0$. These two limits are illustrated by the solid and open circles, respectively, in Figure 10.

We conclude that brightest galaxies not being at the center of their host clusters, and having large velocities, is a transient phenomenon, closely associated to major mergers between clusters. If the last major merger took place at large redshift, $z \gtrsim 0.3$ (or if no such merger ever took place), the cluster has time to reach equilibrium before the present. But if the last major merger took place recently, the cluster will still be out of equilibrium at $z = 0$. This explains why f_{BNC} increases with cluster mass: low-mass clusters are the ones that have not experienced any major merger in their recent history. They formed at high redshift, and were “left alone” until the present, giving them time to reach equilibrium.

All calculations were performed at the Laboratoire d’astrophysique numérique, Université Laval. This work benefited from stimulating discussions with Benoit Côté, Roger Coziol, Heinz Andernach, Cesar Augusto Caretta, an anonymous referee, and especially Ramin Skibba, who also provided some of the data plotted in Figure 2. We are pleased to acknowledge the support of the Canada Research Chair program, NSERC, and the Stages Sigma+ program at Université Laval. PB acknowledges support from the FP7 ERC Starting Grant “cosmoIGM.”

REFERENCES

- Abell, G. O., Corwin, H. G. Jr., & Oowin, R. P. 1989, *ApJS*, 70, 1
- Adami, C., Biviano, A., Durret, F., & Mazure, A. 2005, *A&A*, 443, 17
- Adernach, H., & Coziol, R. 2007, in *ESO Astrophysics Symp., Groups of Galaxies in the Nearby Universe*, ed. I. Saviane, V. Ivanov, & J. Borissova (New York:Springer), 379 (astro-ph/0603295)
- Azzaro, M., Patiri, S. G., Prada, F., & Zentner, A. R. 2007, *MNRAS*, 376, 43
- Bahcall, N. A., & Cen, R. 1993, *ApJ*, 407, L49
- Barai, P., Brito, W., & Martel, H. 2009, *JA&A*, 30, 1
- Baugh, C. M. 2006, *Rep.Prog.Phys.*, 69, 3101
- Beers, T. C., & Geller, M. J. 1983, *ApJ*, 274, 491
- Behroozi, P. S., Conroy, C., & Wechsler R. H. 2010, *ApJ*, 717, 379
- Berlind, A. A. et al. 2006, *ApJS*, 167, 1
- Bildfell, C., Hoekstra, H., Babul, A., & Mahdavi, A. 2008, *MNRAS*, 389, 1637
- Bird, C. M. 1994, *AJ*, 107, 1637
- Cacciato, M., van den Bosch, F. C., More, S., Li, R., Mo, H. J., & Yang, X. 2009, *MNRAS*, 394, 929
- Cohn, J. D., Kochanek, C. S., McLeod, B. A., & Keeton, C. R. 2001, *ApJ*, 554, 1216
- Cole, S., Lacey, C. G., Baugh, C. M., & Frenk, C. S. 2000, *MNRAS*, 319, 168
- Cooray, A. 2005, *MNRAS*, 363, 337
- Coziol, R., Andernach, H. Caretta, C. A., Alamo-Martinez, K. A., & Tago, E. 2009, *AJ*, 137, 4795
- Coziol, R., & Plauchu-Frayn, I. 2007, *AJ*, 113, 2630
- Croton, D. J. et al. 2006, *MNRAS*, 365, 11
- De Lucia, G., & Blaizot, J. 2007, *MNRAS*, 375, 2
- Díaz, E., Zandivarez, A., Merchán, M. E., & Muriel, H. 2005, *ApJ*, 629, 158
- Dutton, A. A., Conroy, C., van den Bosch, F. C., Prada, F., & More, S. 2010, *MNRAS*, 407, 2
- Ellingson, E. 2003, *Ap&SS*, 285, 9

- Guo, Q. et al. 2011, MNRAS, 413, 101
- Hatton, S., Devriendt, J. E. G., Ninin, S., Bouchet, F. R., Guiderdoni, B., & Vibert, D. 2003, MNRAS, 343, 75
- Haussman, M. A., & Ostriker, J. P. 1978, ApJ, 224, 320
- Hwang, H. S., & Lee, M. G. 2008, ApJ, 676, 218
- Johnston, D. E. et al. 2007, preprint (arXiv:0709:1159)
- Kauffmann, G., White, S. D. M., & Guiderdoni, B. 1993, MNRAS, 264, 201
- Killedar, M., Borgani, S., Meneghetti, M., Dolag, K., Fabjan, D., & Tornatore, L. 2012, MNRAS, 427, 533
- Kimm, T. et al 2009, MNRAS, 394, 1131
- Kochanek, C. S. 1995, ApJ, 445, 559
- Koester, B. P. et al. 2007, ApJ, 660, 239
- Koopmans, L. V. E., & Treu, T. 2003, ApJ, 583, 606
- Li, R., Mo, H. J., Fan, Z., Yang, X., & van den Bosch, F. C. 2013, MNRAS, 430, 3359
- Lin, Y.-T., & Mohr, J. J. 2004, ApJ, 617, 879
- Lo Farom, B., Monaco, P., Vanzella, E., Fontanot, F., Silva, J., & Cristiani, S. 2009, MNRAS, 399, 827L
- Malumuth, E. M. 1992, ApJ, 386, 420
- Malumuth, E. M., Kriss, G. A., Van Dyke Dixon, W., Fergusson, H. C., & Ritchie, C. 1992, AJ, 104, 495
- Mandelbaum, R., Seljak, U., Kauffmann, G., Hirata, C. M., & Brinkmann, J. 2006, MNRAS, 368, 715
- Martel, H., Barai, P., & Brito, W. 2012, ApJ, 757, 48
- Matsuoka, Y., Masaki, S., Kawara, K., & Sugiyama, N. 2011, MNRAS, 410, 548
- McKay, T. A. et al. 2002, ApJ, 571, L85
- Merritt, D. 1984, ApJ, 276, 26
- Merritt, D. 1985, ApJ, 289, 18

- Mihos, J. C. 2004, in *Carnegie Obs. Astrophys. Ser., Clusters of Galaxies: Probes of Cosmological Structure and Galaxy Evolution*, ed. J. S. Mulchaey, A. Dressler, & A. Oemler (Cambridge: Cambridge Univ. Press), 277
- Monaco, P., Fontanot, F., & Taffoni, G. 2007, *MNRAS*, 375, 1189
- More, S., van den Bosch, F. C., Cacciato, M., Mo, H. J., Yang, X., & Li, R. 2009, *MNRAS*, 392, 801
- More, A., Cabanac, R., More, S., Alard, C., Limousin, M., Kneib, J.-P., Gavazzi, R., Motta, V. 2012, *ApJ*, 749, 38
- Oegerle, W. R., & Hill, J. M. 2001, *AJ*, 122, 2858
- Oguri, M. 2006, *MNRAS*, 367, 1241
- Ostriker, J. P., & Tremaine, S. D. 1975, *ApJ*, 202, L113
- Pastor Mira, E., Hilbert, S., Hartlap, J., & Schneider, P. 2011, *A&A*, 531A, 169
- Phleps, S., Peacock, J. A., Meisenheimer, K., & Wolf, C. 2006, *A&A*, 457, 145
- Pimbblet, K. A., Roseboom, I. G., & Doyle, M. T. 2006, *MNRAS*, 368, 651
- Postman, M., & Lauer, T. R. 1995, *ApJ*, 440, 28
- Prescott, M. et al. 2011, *MNRAS*, 417, 1374
- Reid, B. A. & Spergel, D. N. 2009, *ApJ*, 698, 143
- Richardson, J., Zheng, Z., Chatterjee, S., Nagai, D., & Shen, Y. 2012, *ApJ*, 755, 30
- Romanowsky, A. J., Strader, J., Spitler, L. R., Johnson, R., Brodie, J. P., Forbes, D. A., & Ponman, T. 2009, *AJ*, 137, 4956
- Rusin, D. et al. 2003, *ApJ*, 587, 143
- Sanderson, A. J. R., Edge, A. C., & Smith, G. P. 2009, *MNRAS*, 398, 1698
- Scoccimarro, R., Sheth, R. K., Hui, L., & Jain, B. 2001, *ApJ*, 546, 20
- Sheldon, E. S. et al. 2009, *ApJ*, 703, 2232
- Sheth, R. K., Hui, L., Diaferio, A., & Scoccimarro, R. 2001, *MNRAS*, 325, 1288
- Skibba, R. A., van den Bosch, Yang, X., More, S., Mo, H., & Fontanot, F. 2011, *MNRAS*, 410, 417
- Somerville, R. S., Hopkins, P. F., Cox, T. J., Robertson, B. E., & Hernquist, L. 2008, *MNRAS*, 391, 481

- Springel, V., White, S. D. M., Tormen, G., & Kauffmann, G. 2001, *MNRAS*, 328, 726
- Springel, V. et al. 2005, *Nature*, 435, 629
- Taylor, J. E., & Babul, A. 2004, *MNRAS*, 348, 811
- Tinker, J. L., Conroy, C., Norberg, P., Patiri, S. G., Weinberg, D. H., & Warren, M. S. 2008, *ApJ*, 686, 53
- van den Bosch, F. C., Norberg, P., Mo, H. J., & Yang, X. 2004, *MNRAS*, 352, 1302
- van den Bosch, F. C., Weinmann, S. M., Yang, X., Mo, H. J., Li, C., & Jing, Y. P. 2005, *MNRAS*, 361, 1203
- van den Bosch, F. C. et al. 2007, *MNRAS*, 376, 841
- van Uitert, E., Hoekstra, H., Schrabback, T., Gilbank, D. G., Gladders, M. D., Yee, H. K. C. 2012, *A&A*, 545A, 71
- von der Linden, A., Best, P. N., Kauffmann, G., & White, S. D. M. 2007, *MNRAS*, 379, 867
- Watson, D. F., Berlind, A. A., McBride, C. K., Hogg, D. W., & Jiang, T. 2012, *ApJ*, 749, 83
- Weinmann, S. M., van den Bosch, F. C., Yang, X., & Mo, H. J. 2006, *MNRAS*, 366, 2
- Wetzel, A. R., Tinker, J. L., Conroy, C., & van den Bosch, F. C. 2013, *MNRAS*, 432, 336
- Woo, J. et al. 2013, *MNRAS*, 428, 3306
- Yang, X., Mo, H. J., & van den Bosch, F. C. 2003, *MNRAS*, 339, 1057
- Yang, X., Mo, H. J., van den Bosch, F. C. & Jing, Y. P. 2005, *MNRAS*, 356, 1293
- Yang, X., Mo, H. J., van den Bosch, F. C., Pasquali, A., Li, C., & Barden, M. 2007, *ApJ*, 671, 153
- Yang, X., Mo, H. J., van den Bosch, F. C.; Bonaca, A., Li, S., Lu, Yi, Lu, Yu, & Lu, Z. 2013, *ApJ*, 770, 115
- Yoshikawa, K., Jing, Y. P., & Börner, G. 2003, *ApJ*, 590, 654
- Zehavi, I. et al. 2005, *ApJ*, 630, 1
- Zheng, Z. et al. 2005, *ApJ*, 633, 791
- Zabludoff, A. I., Geller, M. J., Huchra, J. P., & Vogeley, M. S. 1993, *AJ*, 106, 1273
- Zabludoff, A. I., & Mulchaey, J. S. 1998, *ApJ*, 496, 39